Review

Israel Journal of Chemistry

DOI: 10.1002/ijch.201400091

A Nanochannel Platform for Single DNA Studies: From Crowding, Protein DNA Interaction, to Sequencing of Genomic Information

Johan R. C. van der Maarel,* Ce Zhang, and Jeroen A. van Kan[a]

Abstract: The study of nanochannel-confined DNA is important from biotechnological and biophysical points of view. We produce nanochannels in elastomer with soft lithography and proton beam writing. Issues concerning DNA confined in such quasi one-dimensional channels are discussed. We describe DNA stretching via the control of channel diameter and buffer conditions and how the extension can be interpreted with theory and computer simulation. We then discuss the conformation of nano-confined DNA crowded by neutral polymers and like-charged proteins. As an example of a protein that has an affinity to DNA, the effect of heat-stable nucleoid-structuring protein, H-NS, on the folding and compaction of DNA is reviewed. Compaction of DNA by eukaryotic protamine and unpacking of pre-compacted DNA through an increase in salt concentration are discussed. We review results obtained with a novel, cross-channel device that allows the monitoring of the dynamic, conformational response of DNA after exposure to a ligand or protein and/or a change in buffer conditions *in situ*. As a biotechnological application, linearization of DNA by bottle-brush coating with a polypeptide copolymer is discussed. It is demonstrated that large-scale genomic organization can be sequenced using single DNA molecules on an array of elastomeric nanochannels. Overall, our results show that the effects of ligands and proteins on the conformation, folding, and condensation of DNA are not only related to classical controlling factors, such as osmotic pressure, charge, and binding, but that the interplay with confinement in a nanospace is of paramount importance.

Keywords: DNA · DNA condensation · gene sequencing · nanofluidics · nanoparticles

1. Introduction

Advances in nanolithography have made it possible to fabricate nanofluidic devices with at least one dimension of around a few tens of nanometers. Nano-devices featuring entropic trap arrays, pillar arrays, pores, or channels have been designed and used for the analysis of the properties of long biopolymers, including DNA.[1–4] Here, we discuss long and straight quasi one-dimensional channel devices with cross-sectional diameters of tens to hundreds of nanometers. Within such a nanochannel, a single DNA molecule or nucleoprotein complex can be confined and visualized with fluorescence microscopy. The nanofluidic devices are hence complementary to other single-molecule manipulation techniques, such as those based on tweezers.[5,6] An important difference is that the confinement experiment does not require chemical modification to attach the biomolecule to molecular pincers. The molecules can hence be investigated closer to their native state. Confinement is important in certain biological processes, such as DNA packaging in viruses, or segregation of DNA in bacteria.[7,8] Accordingly, besides single-molecule manipulation, nanochannels serve as a model system for the investigation of the compaction of DNA in a nanospace, in conjunction with other important compaction modes, such as macromolecular crowding and/or binding of condensing proteins or ligands.

The opportunity to investigate single molecules inside nanochannels has stimulated fundamental research as to the effects of channel diameter,[9,10] and salt concentration, on the conformation of DNA.[11–14] Other studies have focused on the dynamics, to elucidate the variation in the extension due to thermal fluctuation,[15] or the response of the molecular motion to entropic, electrophoretic, and frictional forces.[16] The conformation and dynamics of DNA in confinement have also been investigated with computer simulation.[17–20] These simulations contribute to our understanding of the different physical mechanisms at play. Besides fundamental studies, nanochannels are important for biotechnological applications,

[a] J. R. C. van der Maarel, C. Zhang, J. A. van Kan
Department of Physics
National University of Singapore
117542 (Singapore)
e-mail: johanmaarel@gmail.com

such as mapping of large-scale genomic organization with restriction enzyme cutting, nick labeling, or denaturation mapping.[21–24] Advantages of the nanochannel platform are that the DNA molecules are in an equilibrium conformation; high throughput can be achieved by using arrays of parallel channels and integration with lab-on-chip devices. Future devices might involve non-equilibrium translocation of DNA molecules through a pore, or by a sensor, a process that can be facilitated by a nanochannel platform.[25]

The fundamentals of confinement and linearization of DNA, including the effects of channel diameter and buffer ionic strength, as well as various biotechnological applications, have been reviewed before.[26,27] In the present review, we merely summarize our own contributions, in the context of macromolecular crowding and protein/polypeptide DNA interaction. The organization of this review is as follows: we start with a brief presentation of our channel devices, which are made of elastomer and fabricated with soft lithography.[28] To illustrate our experimental procedures, we then describe stretching of DNA, by means of control of channel diameter and buffer conditions, and how the extension can be interpreted with theory and computer simulation. As a first example of a surprising effect of confinement on an important biophysical phenomenon, we discuss the compaction of nano-confined DNA crowded by neutral polymer or like-charged protein.[29,30] This is followed by a study of heat-stable nucleoid-structuring protein (H-NS), an electroneutral protein that plays a role in the folding and compaction of DNA in the nucleoid of a bacterial cell.[31] We review results obtained with a novel, cross-channel device, which allows the monitoring of the dynamic, conformational response of DNA after exposure to a binding or non-binding ligand or protein and/or a change in environmental solution conditions *in situ*.[32] As an example of a cationic condensing agent involved in spermiogenesis, we discuss the compaction of DNA with protamine and the unpacking of protamine pre-compacted DNA through an increase in salt concentration. Eventually, we review linearization of DNA by bottlebrush coating with a polypeptide copolymer.[33] In particular, it will be demonstrated that large-scale genomic organization can be sequenced using single DNA molecules on an array of nanochannels made of elastomer and produced with soft lithography.

Johan van der Maarel was born in 1960 in Maassluis, The Netherlands. He received his Ph.D. in physical chemistry from Leiden University in 1987. His doctoral work was on the structure and dynamics of water and aqueous solutions. He was employed at Leiden University as Lecturer in Physical and Macromolecular Chemistry until 2004. He then moved to the National University of Singapore as Associate Professor in Biophysics. His research is concerned with nanofluidics, but he also applies nuclear magnetic resonance, computer simulation, microrheology, and scattering methods to complex fluid systems. He has been carrying out studies of, among others, polyelectrolytes including DNA, ionic copolymers, and meso-structures of DNA.

Ce Zhang was born in 1979 in Liaoning, China. He conducted his graduate studies at the National University of Singapore. His doctoral work was on the conformation and dynamics of single DNA molecules confined in a nanospace. After graduation with a Ph.D. degree in physics in 2009, he was employed as a postdoctoral researcher at the Department of Medical Biochemistry and Biophysics, Umea University, and studied the assembly of Alzheimer's disease related proteins and peptides. He moved back to Singapore in 2010 and continued his research on proteins and DNA in nano-confinement.

Jeroen van Kan was born in 1969 in Utrecht, The Netherlands. He received his Ph.D. in physics from the Free University, Amsterdam in 1996. In 2007, he received the Institute of Physics Singapore, Omicron Nanotechnology Award. Currently, he is an Associate Professor in the Department of Physics at the National University of Singapore. In his research, he employs fast light ions for lithography and analysis. In his research group, new methods are developed for next generation 3D nanolithography via direct write and nanoimprint lithography, with an emphasis on the manufacturing of nanofluidic lab on chip devices in polymer substrates. He has developed the technology for the fabrication of nanofluidic polymer lab-on-chip devices.

2. Fabrication of Nanofluidic Devices

Devices with at least one dimension in the range of nanometers can be fabricated in glass, silicon, or plastics.[26,27] Our devices are produced by soft lithography and made of polydimethylsiloxane (PDMS).[28] Elastomer chips have some advantages, including the possibility of obtaining multiple replicas by casting on a master stamp. We cast about one hundred replicas with a single stamp, so that a fresh chip is used for every experiment. The channels are quasi one-dimensional, with a rectangular cross-section of tens to hundreds of nm, and a length of around 50 μm. Furthermore, they are arranged in either a single array of parallel channels, or two intersecting arrays of channels in a perpendicular configuration.[32] For an illus-

Israel Journal of Chemistry

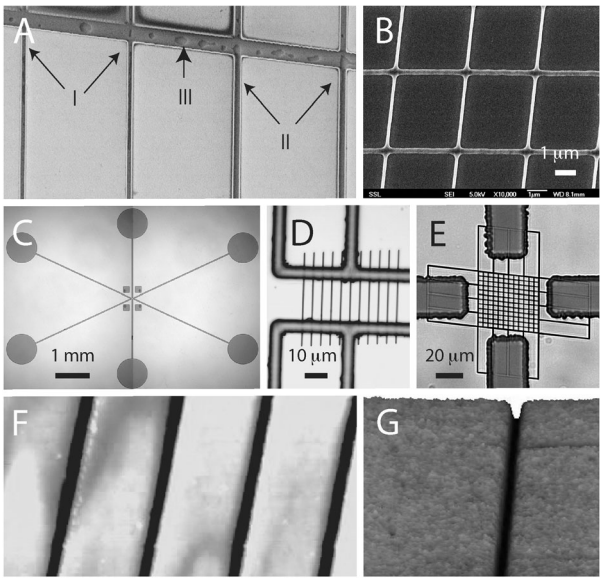

Figure 1. (A) Scanning electron microscopy image of the HSQ master stamp, showing a positive standing channel structure with a width of 150 (I) and 200 (II), and a uniform height of 300 nm. Feature III is a 500 nm wide feeder channel. (B) As in panel (A), but for a crossed-channel structure with widths of 250 and 150 nm, and a uniform height of 200 nm. The wide and narrow channels are laid on a rectangular grid and separated by 4.0 and 3.75 µm, respectively. (C) Bright field optical image of the bonded lab-on-chip, cross-channel device. The loading reservoirs (1 mm diameter) are connected to the central grid of nanochannels by microchannels in SU-8 resin. (D) Zoom of a single array of nanochannels with connecting microchannels. (E) Zoom of two arrays of nanochannels in crossed configuration. (F) Atomic force microscopy image of the PDMS replica, showing an array of parallel channels, with a width and depth of 200 and 300 nm, respectively. (G) As in panel (F), but for a single channel, with a width and depth of 105 and 100 nm, respectively.

tration of the typical layout of our devices, see Figure 1. Nanochannel-patterned master stamps are made in hydrogen silsesquioxane (HSQ) resist using a lithography process, with MeV proton beam writing. Exposing HSQ resist material, with fast protons, guarantees accurate lateral control of energy deposition in the resist. After chemical development of the HSQ resist, smooth and well-defined details in the master stamp are obtained. This technique is capable of writing details down to sub-20 nm in resist material, with side-wall smoothness down to 2–3 nm rms.[34–36] A superposing set of feeding microchannels, which are connected to (the arrays) of nanochannels, is made in epoxy-based SU-8 resist with UV lithography (365 nm). The width and height of the ridges in the master stamp are measured by scanning electron and atomic force microscopy, respectively, and verified by ionic conductivity measurements. To guarantee long stamp life and accurate PDMS replication, a Teflon coating is applied on the master stamp.[37] The PDMS elastomer is SylgardTM 184 (Dow Corning Co.), and the PDMS base and curing agent are mixed in a ratio of 10 : 1. After curing and release from the master stamp, holes are punched to form reservoirs for loading the reagents. The replica is then sealed with a glass coverslip, after both have been plasma oxidized. The accurately defined details of the stamp prevent collapse of the replicated PDMS nanofluidic structure. One side of the channels is lined by glass, but a full elastomer-lined channel can be fabricated, if a layer of PDMS is spin-coated on the coverslip prior to plasma oxidation and bonding.

3. DNA Stretching

In most experiments, bacteriophage λ DNA (48.5 kbp) or T4 DNA (166 kbp) molecules are brought into an array of nanochannels, by either the application of an electric field, or by pressurized injection. Once the molecules are inside the channels, the electric field, or applied pressure, is removed, and the molecules relax to an equilibrium state. The relaxation time is a few seconds to a minute, depending on environmental solution conditions.[15,16] The whole process of loading, equilibration, and eventual elongation, or compaction, of the DNA molecules can be monitored with fluorescence microscopy. However, to visualize the DNA molecules, it is necessary to stain them with a dye. A commonly employed dye is YOYO-1, which bis-intercalates between three adjacent base-pairs, with a concomitant increase in DNA contour length.[38,39] The maximum level of intercalation is four base-pairs per dye molecule. Furthermore, YOYO-1 carries four positive charges, so that it also partially neutralizes the DNA phosphate charge (for maximum loading, the DNA charge is thus reduced by a factor of two). For a minimal distortion of the DNA secondary structure, minimal reduction of the DNA net charge, and minimal photo damage, it is advisable to use a minimal level of staining. In a buffer of low ionic strength (a few mM), a level of intercalation of about 25 base-pairs per YOYO-1 molecule results in a sufficiently intense fluorescence signal for accurate imaging.[13] The YOYO-1 to base-pair ratio needs, however, to be increased at higher ionic strength, because of decreased binding of YOYO-1 on DNA by increased screening of the Coulomb interaction.

In most nanofluidic experiments, DNA molecules are incubated with the relevant buffer for a period of time (24 h) before they are brought into channels of various cross-sectional diameter. We have employed two different buffer systems: Tris-borate/EDTA (TBE) and Tris/HCl (T). TBE buffer contains some multivalent ions, but at pH 8.5 their concentrations are vanishingly small (1× TBE is 90 mM Tris, 90 mM boric acid, and 2 mM EDTA, pH 8.5). The T buffer system contains monovalent ions only (1×T is 2.9 mM TrisCl and 7.1 mM Tris, pH 8.5). A montage of fluorescence images of single λ DNA molecules, confined in rectangular channels with various cross-

sectional dimensions in 5×TBE, is shown in Figure 2A. Another montage of images of T4 DNA in 300×300 nm^2 channels, and various concentrations of TBE buffer, is shown in Figure 2C. Note that differences in width and brightness between molecules of similar extension are related to effects of photo-bleaching and have no physical meaning. The equilibrated stretch in the longitudinal direction of the channel depends on the concentration of the buffer and/or diameter of the channel. With decreasing channel diameter and/or decrease in buffer concentration, the molecules take a more extended conformation.[9–11,13]

The extension of the DNA molecules confined in the nanochannels can be determined from the fluorescence intensity profile. Since these are essentially single-molecule experiments, it is advisable to measure a large number of molecules (tens to hundreds) for each experimental condition. An example of a typical distribution in extension, using a pool of 1000 molecules, is shown in Figure 2E. The distribution is close to Gaussian, but is skewed towards the smaller values of extension. This is due to the presence of a small fraction of DNA fragments generated by sample handling and (photo) damage. These fragments should be ignored in the calculation of the mean value of the extension. For the cut-off, we use the mean value minus two times the standard deviation. The mean relative extensions, $R_{\parallel}/L$, i.e., the mean extensions divided by the contour length of the molecule, are set out in panels B and D of Figure 2. Note that the maximum extension of the DNA molecules inside the channels is about 40% of the contour length. This implies that in the present environmental conditions, the molecules are always locally coiled, irrespective of channel diameter and concentration of salts.

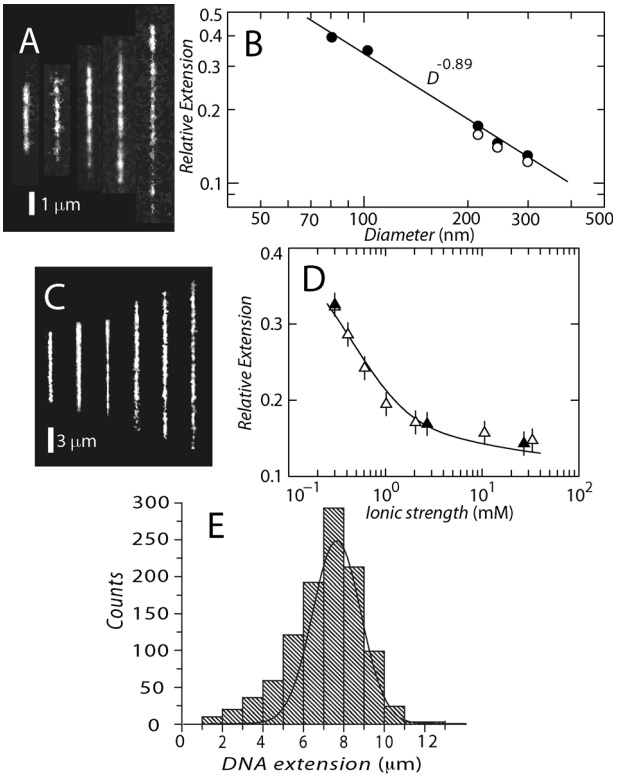

Figure 2. (A) Montage of fluorescence images of λ DNA in 5× TBE buffer (pH 8.5). The channel cross-sections are 300×300, 200×300, 150×300, 100×105, and 100×60 nm^2, from left to right. (B) Mean values of the relative extension. The closed and open symbols refer to λ DNA and T4 DNA, respectively. The solid line represents the scaling law for a locally coiled polymer in a tube. (C) Fluorescence images of T4 DNA in 300×300 nm^2 channels. The buffer concentration decreases, from left to right, according to 1, 1/15, 1/30, 1/50, 1/75, and 1/100×TBE. (D) Relative extension of T4 DNA in 300×300 nm^2 channels versus solvent ionic strength. The open symbols refer to TBE buffer conditions, whereas the closed symbols pertain to the T buffer system. The solid curve represents a fit of the theoretically predicted extensions, based on the blob model.[13] (E) Distribution in relative extension of T4 DNA in 5× TBE buffer (pH 8.5). The channel cross-section is 300×300 nm^2. The solid line denotes a Gaussian fit. Panels A–D are reproduced by permission of The American Institute of Physics from Refs. [13, 28].

In a nanochannel, a linear biomolecule elongates because of the restriction in configurational degrees of freedom imposed by the channel walls. This effect is similar to the situation in a single-molecule stretching experiment, in which the biomolecule is subjected to a tensional force. The role of the strength of the stretching force is the same as the value of the cross-sectional diameter of the nanochannel, in the sense that both a stronger force and a decrease in diameter result in a more extended conformation. For wider channels, the effective stretching force is thermal energy divided by channel diameter, so that confinement inside a channel of 200 nm corresponds to stretching the molecule with a force of around 0.02 pN.[40] The statistics of a DNA molecule confined in a nanochannel depends on the ratio of the channel diameter to the DNA persistence length. Another important factor is the interaction of spatially close segments, which are separated over a long distance along the contour of the DNA molecule (excluded volume or self-avoidance). Inside relatively wide channels, but with a width less than the radius of gyration of the unconstrained, free DNA molecule, the molecule remains coiled at all length scales (blob regime; see illustration in Figure 3A). The statistics can then be described with scaling theory, including the effects of bending rigidity (persistence length) and self-avoidance (excluded volume).[41,42] On the other hand, inside a very narrow channel, with a width less than the persistence length, the DNA molecule undulates, and only bends when it bounces off the wall (deflection regime).[43] In the transition regime, with a channel diameter of a few times the persistence length, the statistics is more complicated and not readily amenable to simple scaling theory. Notably, most reported works on bare DNA involve the transition and blob regimes. To linearize bare DNA beyond an extension of about 80% of its contour length into the deflection regime, the channel di-

Israel Journal of Chemistry

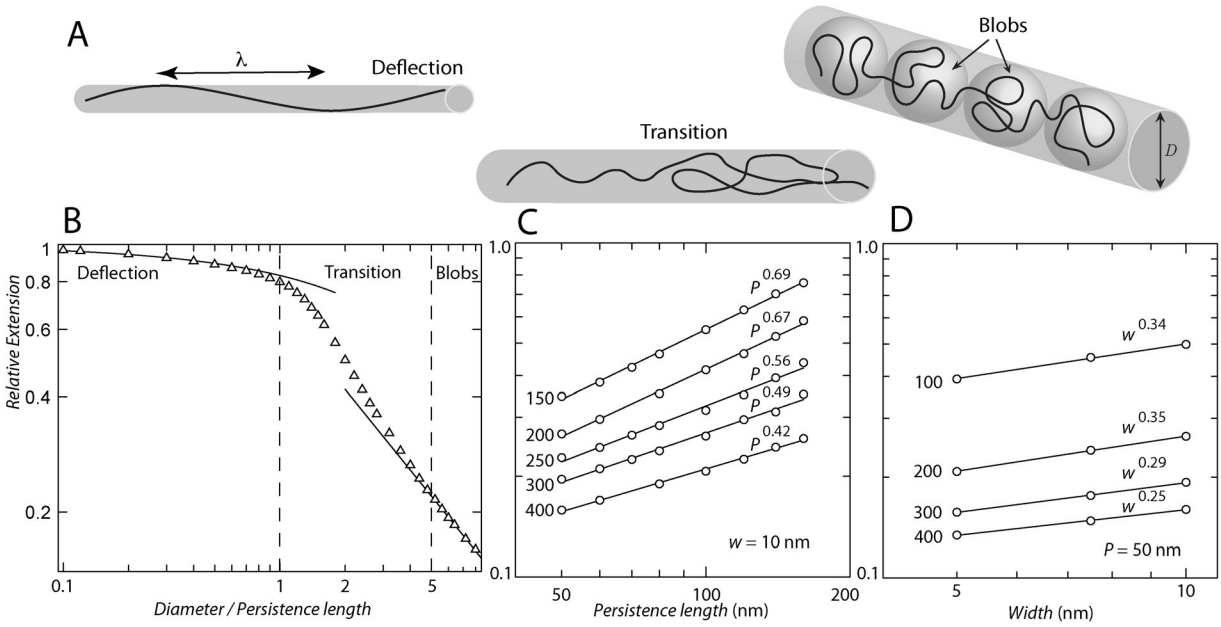

Figure 3. (A) Schematic conformation of a deflecting worm in a narrow channel (left), a back-folded worm in a channel with intermediate diameter (middle), and a locally coiled worm as an array of blobs in a wider channel (right). (B) Monte Carlo results of the relative extension versus channel diameter divided by persistence length (50 nm). The chain width $w = 10$ nm and contour length $L = 8$ μm. The curves represent deflection and blob theories.[50] (C) Monte Carlo results of the relative extension versus persistence length for a chain with $w =$ 10 nm. (D) As in panel (C), but for the relative extension versus w for a chain with $P = 50$ nm. The channel diameters and fitted scaling exponents are indicated. Panels C and D are reproduced by permission of The Royal Society of Chemistry from Ref. [31].

ameter needs to be reduced to a value of less than 50 nm. Such extremely narrow channels are not easily fabricated in elastomers, but they can be produced in fused silica.[15,16,44] Folded structures of lengths 150–250 nm have been observed for DNA confined in channels with a diameter of around 100 nm.[45]

4. Scaling Theory and Monte Carlo Simulation

In Daoud and de Gennes' scaling approach for a worm in a wider channel, the molecule is considered as a linear sequence of sub-coils of uniform size.[41,42] These sub-coils are commonly referred to as blobs. Within the blobs, the DNA molecule is thought to be unaffected by the presence of the channel walls. Furthermore, self-avoidance is screened beyond the blob size, because segments pertaining to different blobs cannot form contact pairs. Successive blobs have a second virial coefficient of repulsive interaction of the order of their volume and, hence, they are packed into a linear array. For a self-avoiding, worm-like chain with persistence length, P, and width, w, in a wide channel with diameter $D \gg P$, the blob model predicts a scaling law for the relative extension

$$R_{\parallel}/L \propto D^{-2/3} P^{1/3} w^{1/3} \qquad (1)$$

In particular, the scaling exponent for both P and w is predicted to be 1/3. A variation in extension, close to $\propto D^{-2/3}$, for DNA molecules confined in nanochannels of various diameter, has been experimentally confirmed (see, for instance, Figure 2B).[10,27] The variation in extension with the ionic strength of the supporting medium has been interpreted with a modified version of the blob model, including a variation in persistence length, P, and effective diameter, w, of the duplex, through screening of the Coulomb interaction (Figure 2D).[13]

In Odijk's deflection regime for a worm in a very narrow channel (that is, $D < P$), the molecule is undulating, since it is deflected by the walls.[43] As a result of the undulation with deflection length $\lambda \sim D^{2/3} P^{1/3}$, $R_{\parallel}/L$ is reduced with respect to its fully stretched value of unity according to

$$R_{\parallel}/L = 1 - c(D/P)^{2/3}, \qquad (2)$$

with $c = 0.1701$ for a circular cross-section.[46] Notably, the deflection theory is quantitative, since it includes the pre-factor in the expression for the extension. In the blob model, the pre-factor is unknown, so that no quantitative information regarding P and w can be derived from the experimental values of the stretch. Furthermore, as shown by a comparison with Monte Carlo computer simulation results (Figure 3B), the range of applicability of the theoretical models does not cover the experimentally

important transition regime with D/P from 1 to 5 (that is, $D = 50$–250 nm). Several theoretical attempts have been reported to bridge the gap. For the chain to cross over from the blob regime, the blob size reduces, such that the volume interaction energy per blob becomes less than the thermal energy, kT. This results in modified, or the same, scaling of $R_{\|}/L$ with D, depending on the presumed chain statistics within the blob.[13,18,47] On the other hand, for the crossover from the deflection regime, the chain starts to loop, and exhibits back-folded hairpin conformations.[48–50]

Monte Carlo computer simulation of a wormlike chain confined in nanochannels of various diameter provides quantitative information regarding the stretch, in terms of persistence length, P, and diameter, w.[50,47] The Monte Carlo simulation results for $R_{\|}/L$ as a function of P, for fixed $w = 10$ nm, as well as $R_{\|}/L$ as a function of w, for fixed $P = 50$ nm, are shown in panels C and D of Figure 3, respectively.[31] To a good approximation, the extension follows a power law in P and w; that is, $R_{\|}/L \propto P^{\alpha} w^{\beta}$. The fitted values of the exponent, α, depend on the value of the tube diameter, D. Only for rather wide channels, with $D = 400$ nm, the simulation result for α approaches the prediction of blob theory (1/3, see Eq. 1). On the other hand, the simulation results for β are always close to the value given by the blob model, irrespective of channel diameter. As will be shown below, we have used the simulated scaling exponent, α, for the interpretation of the increase in stretch, following filamentation of DNA and formation of a nucleoprotein complex by the binding of a bacterial protein. We have used the simulated stretch-diameter curve for the interpretation of the linearization of DNA bottlebrush coated with a polypeptide diblock copolymer. However, we will first describe the effects of crowding agents and like-charged proteins on the conformation of nanochannel-confined DNA.[29,30]

5. Crowding and Confinement

A substantial fraction of the total volume of biological media is occupied by macromolecules that have no specific affinity for one another. However, these essentially inert crowding agents have a profound effect on molecular transport, reaction rates, and chemical equilibrium. Crowding also affects molecular structure and function. A well known example is the transition of DNA to a compact form (condensation) in the presence of over-threshold concentrations of simple neutral polymers and simple salts.[51–53] Condensation of DNA with neutral or like-charged crowding agents has gained attention because of its realized importance in a variety of biological processes, including phase separation in the cytoplasm,[54] and the organization of the nucleoid in bacterial cells.[55] Besides background species, the cytoplasm of most eukaryotic cells contains stationary elements, such as cytoskeletal filaments and lipid membranes. These elements affect macromolecular conformation through confinement in one or two dimensions. Accordingly, macromolecular crowding and confinement are intimately related, and deserve an integrated approach in order to understand their modes of operation and how they couple.

We first review the effects of the generic crowding agent, dextran, on the conformation, folding, and condensation of DNA.[29] The employed dextrans are electroneutral, with radii of gyration $R_g = 2.6$, 6.9, and 17 nm for $M_w = 5$, 50, and 410 kDa, respectively. DNAs were incubated with dextran, stained, electrophoresed into the channels, equilibrated for at least 60 s, and imaged with fluorescence microscopy. A montage of fluorescence images of T4 DNA crowded by dextran and confined in 300×300 nm^2 channels is shown in Figure 4A. The relative extensions pertaining to dextrans of different size are set out against the volume fraction of dextran in Figure 4B. With increasing volume fraction, the DNA molecules initially elongate. This elongation is proportional to volume fraction, rather than concentration of dextran. Once the volume fraction is increased beyond a certain critical threshold value, ϕ^*, the DNA molecules condense into a compact form. Condensed DNA molecules can easily be discerned by their bright fluorescence spots (see Figure 4A). The threshold volume fraction for condensation is approximately proportional to the size of the crowder; that is, $\phi^* \propto R_g$. Note that the employed buffer has a relatively low ionic strength of around 3 mM ($1 \times$T buffer). This ionic strength is markedly lower than the one employed in polymer and salt-induced (psi) condensation of DNA in the bulk phase, which typically exceeds 100 mM.[51,52] In the prevalent buffer conditions, an unconstrained DNA molecule does not condense into a compact form by a crowding agent. The condensation is hence facilitated by confinement inside a nanochannel.

Dextrans are neutral nanoparticles, which can penetrate the interior of the solvent-swollen DNA coil. They do not polymerize or complex on DNA, so that both the elongation and condensation of DNA should be related to entropic effects. The depletion interaction between segments of the DNA molecule is attractive, and is expected to reduce the extension prior to condensation. This is not in accordance with our observations (we have observed contraction of confined DNA crowded by like-charged proteins, see below). A qualitative explanation of the elongation has been proposed, and confirmed with computer simulation.[29,56] This explanation is based on the existence of an interfacial layer next to the channel wall in which the DNA segment density is depleted. The thickness of this layer is of the order of the DNA persistence length; that is, 50 to 100 nm, depending on ionic strength.[40] Dextrans can occupy this interfacial layer, because of their small size of a few nm. Furthermore, the dextran density in the interior of the DNA coil is depleted due to hard-core repulsion. The concomitant difference in nanoparticle density between the interfacial and

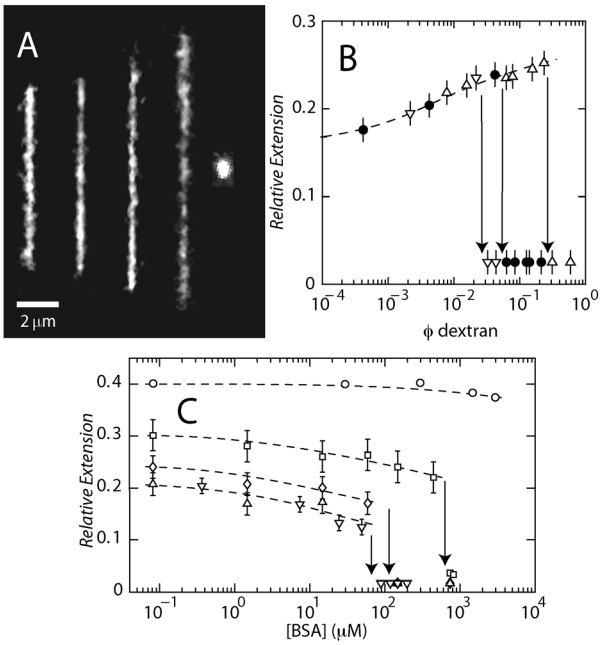

Figure 4. (A) Montage of fluorescence images of T4 DNA in 300× 300 nm^2 channels and 1×T buffer. The molecules are crowded by dextran (R_g=6.9 nm), with volume fraction ϕ=0, 4.2×10^{-4}, 4.2×10^{-3}, 4.2×10^{-2}, and 6.3×10^{-2}, from left to right. The bright spot at the right side represents a condensed molecule. (B) Relative extension of T4 DNA in 300×300 nm^2 channels and 1×T buffer versus the volume fraction, ϕ, of dextran. The dextran R_g=2.6 (▽), 6.9 (●), and 17 (Δ) nm. (C) Relative extension of T4 DNA in 1×T buffer versus the concentration of BSA in 100×60 (○), 100×250 (□), 200×250 (◇), 300×200 (▽), and 300×250 (Δ) nm^2 channels. The dashed curves are drawn as an aid to the eye, and the arrows denote the condensation threshold. Panels A and B are reproduced from Ref. [29]. Panel C is reproduced by permission of the American Chemical Society from Ref. [30].

inner regions of the channel causes an osmotic pressure in the transverse, inward direction. We have estimated that this inward osmotic pressure is sufficient to elongate the chain in the longitudinal direction at the cost of elastic, stretching energy of the DNA molecule.[29]

The condensation phenomenon at an over-threshold volume fraction of crowder is due to depletion-induced attraction between (almost) parallel and juxtaposed DNA segments. Each segment is surrounded by a cylindrical volume from which the crowder is excluded. The diameter of this volume is approximately equal to the sum of the diameter of the DNA duplex and the radius of gyration of the crowder; that is, $D_{DNA}+R_g$. For two parallel cylinders with their center lines of mass separated by a distance, r, with $D_{DNA}<r<D_{DNA}+R_g$, there is an attractive force due to the exclusion of the crowder from the overlap region. Based on an Asakura-Oosawa type of treatment, the interaction energy per unit length is given by the cross-sectional area of the overlap region times the osmotic pressure exerted by crowder, and takes the form

$$\frac{U(r)}{kT} = -\frac{\pi}{4}(D_{DNA}+R_g)^2\left[1-\frac{r}{D_{DNA}+R_g}\right]\rho, \qquad (3)$$

with ρ being the density of the crowder inside the coil.[40,57,58] The attractive depletion interaction is set off against the electrostatic repulsion, leading to a net potential which depends on the relative strengths of the electrostatic repulsion of the like-charged DNA segments and the depletion-induced attraction. Condensation occurs when the absolute value of the depletion interaction energy exceeds a certain critical value. The threshold volume fraction is approximately proportional to the size of the dextran particles, i.e., $\phi^* \propto R_g$, due to the fact that, to leading order, the cross-sectional area of the overlap region is proportional to R_g^2.

Nanoconfinement-facilitated condensation of DNA at relatively low ionic strengths has also been observed for the like-charged proteins bovine serum albumin (BSA, M_w=66.4 kDa, pI=4.9) and hemoglobin (Hb, M_w= 68.0 kDa, pI=7.1).[30] The results for Hb are similar to those pertaining to BSA, and so here, we discuss the results for BSA only. BSA has molecular dimensions of 14×3.8×3.8 nm^3 and has an effective negative charge of −15 at pH 8.5.[59] Its molecular weight and size are hence comparable with the mid-sized dextran, with R_g=6.9 nm. The relative extensions of T4 DNA, crowded by BSA and confined inside channels of various diameter, are set out against the concentration of BSA in Figure 4C. For sub-threshold concentrations of BSA, the molecules are contracted in the longitudinal direction with respect to the protein-free state. This situation is different for dextran, where the molecules were observed to elongate prior to condensation (see Figure 4A). For over-threshold concentrations of BSA and wider channels, condensation of the DNA molecules into a compact form is observed. The critical concentration for condensation shifts to higher values with decreasing cross-sectional channel diameter. In the case of the relatively narrow 60×100 nm^2 channel, the molecules remain stretched, irrespective of BSA concentration. For both dextran and like-charged protein, the threshold concentrations shift to lower values with increasing concentration of salt.[30] The critical concentrations of BSA for condensation are similar to those obtained for dextran, and are in the range of tens to hundreds of μM, depending on the cross-sectional diameter of the channel and the concentration of salts.

BSA and Hb are negatively charged (at pH 8.5), and are not known to have any specific interaction with DNA. Like dextrans, and due to their small size, they are expected to penetrate the interior of the solvent-swollen DNA coil. The protein concentration in the interior of the coil is, however, reduced with respect to the value in the surrounding buffer, due to a combination of electrostatic repulsion and hard-core volume interaction. The like-charged electrostatic repulsion between protein and DNA results in stronger osmotic pressure gradients, as

compared with those generated by the depletion of neutral nanoparticles. For subthreshold concentrations of protein, the osmotic pressure gradient results in contraction of the coil in the longitudinal direction of the channel. The above-described effect of elongation by volume occupancy of nanoparticles next to the channel wall is annihilated, because of the stronger pressure gradients associated with the strong electrostatic repulsion of like-charged protein.

For like-charged proteins, the mechanism for condensation is the same as the one for neutral nanoparticles. A difference is that the cross-sectional diameter of the cylindrical exclusion volume is increased by two times the Debye screening length to account for electrostatic repulsion between DNA and protein. Furthermore, Equation (3) is strictly valid close to the protein theta point; that is, for moderately charged proteins with relatively poor solubility. For proteins of higher charge, higher order cross interactions between DNA and multiple proteins need to be taken into account.[58] This results in increased attraction, but there are no qualitative changes in the distance and orientation dependence of the depletion interaction. An effective attractive interaction requires the juxtaposition of two almost parallel segments. Once the segments are skewed, the overlap region is reduced, and the attraction disappears. The observation that condensation is facilitated by confinement inside a nanochannel can be explained by an increase in contact pairs of almost parallel aligned and juxtaposed segments, due to the DNA segment orientation order imposed by the channel walls. The condensation threshold hence depends on two factors: the orientation order and the probability of a contact. With decreasing cross-sectional diameter, the orientation order increases. Concurrently, the contact probability decreases, because the correlation length of the volume interaction (blob size) is about the diameter of the channel. The increase in threshold with decreasing channel diameter can hence be explained by a decrease in contact probability, despite the increase in orientation order. Once the molecule is fully aligned, no juxtaposed contact pairs can be formed, and condensation is suppressed. Note that dextran and like-charged protein are crowding agents and do not complex or bind on DNA. In the next section, we will discuss the effect of a bacterial protein that has an affinity to DNA.

6. Bacterial Architectural Protein H-NS

Heat-stable nucleoid-structuring protein (H-NS, $M_w =$ 15.6 kDa, pI = 7.5) is involved in gene expression regulation, as well as in the structural organization of the bacterial genome.[60] A fundamental characteristic is that it binds and oligomerizes along double-stranded DNA to form a semi-rigid nucleoprotein filament. As a result of this filamentation, the thermal stability of the duplex is increased and transcription is inhibited.[61,62] Another architectural feature attributed to H-NS is the bridging of distal DNA segments, leading to a reduction in the size of the genome. H-NS mediated bridging has been proposed as a major compaction mode of the bacterial nucleoid.[63] However, net electroneutral H-NS does not behave like a regular condensing agent, such as polyamines or protamine, because it does not condense unconstrained, free DNA into a dense, globular form in physiological buffer conditions.[52] Here, we review the effect of H-NS, in conjunction with confinement inside a nanochannel, on the conformation and compaction of DNA.[31] First, we describe results for DNA molecules that have been pre-incubated with H-NS, in the same way as we have described above for neutral crowders and like-charged proteins. Second, we will discuss the dynamic response of DNA molecules following exposure to H-NS, as obtained with a cross-channel device.

T4 DNA molecules were incubated with a solution of H-NS for at least 24 h, stained, brought into the channels, equilibrated for at least 60 s, and imaged with fluorescence microscopy. We measured the relative extension of the DNA molecules in channels with two different cross-sections: 200×300 and 150×250 nm^2. The results pertaining to 150×250 nm^2 are set out in Figure 5A as a function of the H-NS concentration. The extension depends on the buffer conditions. In a buffer with a moderate ionic strength of a few mM, the DNA molecules elongate with increasing concentration of H-NS. In the case of a buffer with a higher ionic strength of about 40 mM, the molecules are contracted with respect to the protein-free state. For over-threshold concentrations of H-NS, condensation of the DNA molecules into compact forms is observed. Note that for subthreshold concentrations of H-NS, the relative extensions are in the range 0.05–0.4, which implies that the DNA molecules remain solvent-swollen and coiled. In channels with a larger cross-section of 200×300 nm^2, we observed the same qualitative behavior. There are quantitative differences, however, in the values of the stretch and critical concentration of H-NS for condensation (the threshold shifts to a higher value with decreasing channel diameter, as in the case of condensation by crowding). Furthermore, for H-NS, the threshold concentrations are two to three orders of magnitude lower than the ones pertaining to crowding agents.

To obtain more insight in the mechanisms at hand, we have also done experiments with a device featuring two arrays of parallel channels in a crossed configuration (see Figure 1B). With such a device, the conformational response of the DNA molecules to a change in environmental solution conditions can be investigated *in situ*.[32] We have used a buffer with an ionic strength of a few mM, so that equilibrated DNA molecules are either elongated or condensed, depending on the concentration of H-NS. To cover the filamentation and condensation phenomena, we have done a series of experiments with a range of concen-

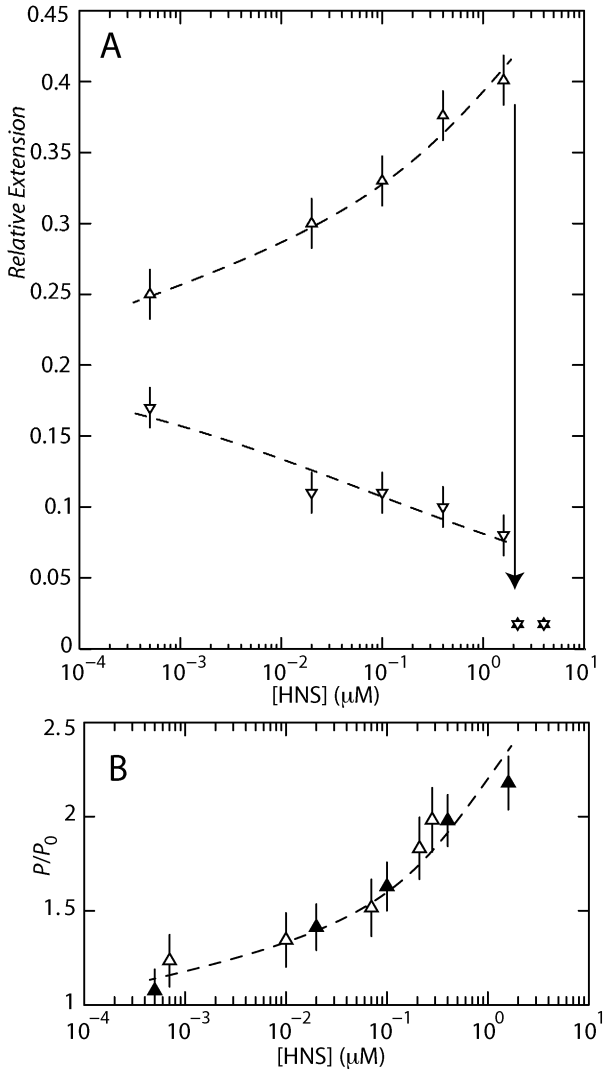

Figure 5. (A) Relative extension of T4 DNA in 1×T buffer with 3 (Δ) or 30 (▽) mM NaCl versus the concentration of H-NS. The molecules are inside 150×250 nm^2 channels. (B) Relative persistence length of T4 DNA in 1×T buffer with 3 mM NaCl and confined in 150×250 (filled symbols) and 200×300 (open symbols) nm^2 channels versus the concentration of H-NS. The dashed line is drawn as an aid to the eye. Panels A and B are reproduced by permission of The Royal Society of Chemistry from Ref. [31].

trations of H-NS across the threshold (0.8–1.6 μM). Protein-free, stained DNA molecules were brought and equilibrated in an array of wider 200×250 nm^2 channels. The buffer containing H-NS was then diffused through the intersecting array of narrower 150×200 nm^2 channels into the wider channels. The buffer exchange was monitored with fluorescence-labeled H-NS and took about 3 s. The stationary DNA molecules were imaged with fluorescence microscopy during exposure to H-NS. As can be seen in the time-lapse series of images and relative extensions in Figure 6A, for a subthreshold concentration of 0.8 μM H-NS, the DNA molecules elongate in a sigmoidal fashion. The molecules reach the final stretch in around 90 min. A series of images captured after exposure to over-threshold concentrations of H-NS (1.0, 1.2, and 1.6 μM), as well as the corresponding relative extensions, are shown in Figure 6B. Now the extensions decrease in

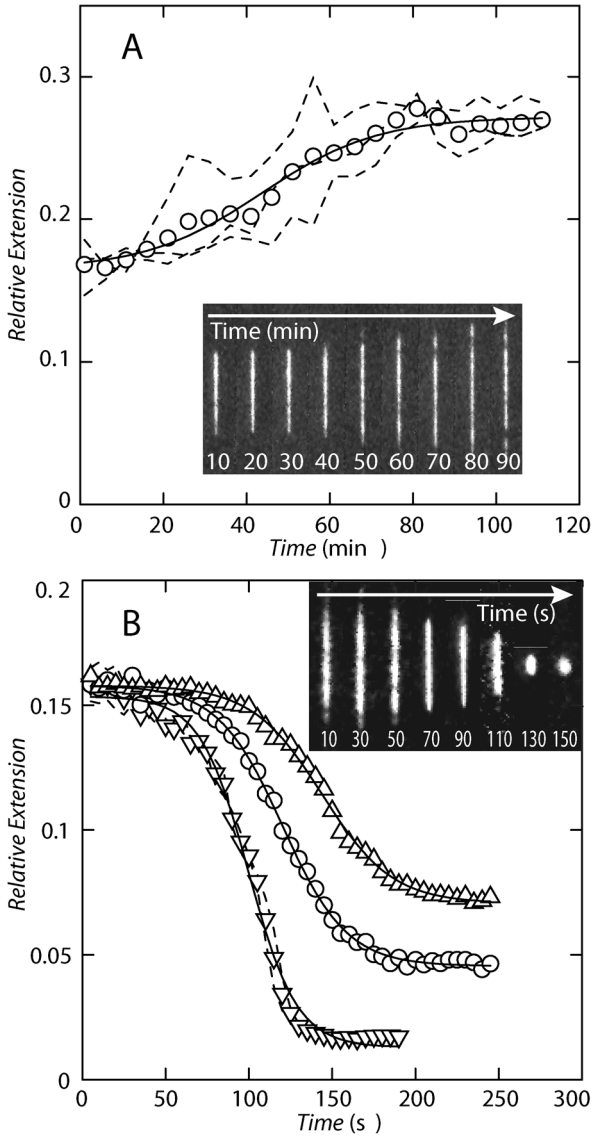

Figure 6. (A) Elongation of T4 DNA following exposure to 0.8 μM H-NS in 1×T buffer and 3 mM NaCl. The molecules are inside 200×250 nm^2 channels. The dashed curves pertain to the elongation of three different molecules and the symbols represent the average. The solid curve represents a sigmoidal fit. The inset shows a time-lapse series of fluorescence images pertaining to a single molecule. (B) Condensation of T4 DNA following exposure to 1.0 (Δ), 1.2 (○), and 1.6 (▽) μM H-NS. The symbols represent averages pertaining to two different molecules for each buffer condition. Individual trajectories are denoted by the dashed curves (1.6 μM H-NS only). The solid curves represent sigmoidal fits. The inset shows a time-lapse series of fluorescence images showing the compaction of a single molecule into the condensed form following exposure to 1.6 μM H-NS. Panels A and B are reproduced by permission of The Royal Society of Chemistry from Ref. [31].

a sigmoidal fashion and, eventually, level off at a level pertaining to the condensed state. The time required for condensation after exposure to H-NS is around a minute. Furthermore, the compaction time and the final extension of the condensates inside the channels depend on the concentration of H-NS, with shorter times and smaller extensions for higher concentrations of H-NS.

With a range of four decades in the H-NS dimer to base pair ratio, we cover the situation with sparsely bound H-NS on DNA to a fully coated filament at H-NS concentrations exceeding 1.0 μM. The observed elongation over a time span of 90 min is due to filamentation, with a concomitant increase in bending rigidity of the nucleoprotein complex. The width of this complex is around 10 nm, as estimated from the diameter of the duplex (2 nm) and the diameter of H-NS (3.5 nm). For a quantitative determination of the persistence length, P, we use the Monte Carlo results for the scaling exponent, α ($w=$ 10 nm). As shown in Figure 3C, α takes the values 0.56 and 0.67 in channels with cross-sectional diameters of 250 and 200 nm, respectively. The increase in P with increasing H-NS concentration can then be obtained from $P/P_o=(R_\parallel/R_\parallel{}^o)^{1/\alpha}$, with P_o and $R_\parallel{}^o$ being the persistence length and stretch for the protein-free state, respectively. The results are shown in Figure 5B. With increasing concentration of H-NS, P increases from the value pertaining to bare DNA (60 nm in 10 mM salt)[6] to about 130 nm just before condensation. This increase in P is in good agreement with the one reported in the literature.[61] Furthermore, the agreement of P obtained for DNA in channels of two different cross-sections confirms the Monte Carlo results for the scaling exponent α and the cancellation of unknown pre-factors in the relevant ratio of the extensions.

In a buffer of higher ionic strength (or with magnesium ions), the DNA molecules are seen to contract with respect to the protein-free state. It should be noted that the concentrations of H-NS are sub-μM and two to three orders of magnitude lower than the ones employed for crowding. Accordingly, depletion of H-NS from the interior of the DNA coil with a concomitant osmotic pressure gradient is not a plausible explanation. Contraction is most likely due to H-NS mediated side-by-side binding of distal segments of the nucleoprotein complex (bridging). In atomic force microscopy and single-molecule manipulation studies, bridging was observed to be induced by divalent ions, such as magnesium and calcium.[64,65] Our nanochannel data show that the onset of bridging is also controlled by screened electrostatics through a variation in the concentration of salts. At low ionic strength of a few mM, effective formation of bridges is prevented by the relatively strong electrostatic repulsion among like-charged DNA segments.

A unique feature of nano-confinement is DNA condensation. Net electroneutral H-NS does not condense DNA in the bulk phase nor in the feeding microchannels of our lab-on-chip device. In the nanochannels, the threshold concentration is around 1 μM, which corresponds with a fully coated filament. The threshold for the filament (pre-incubated DNA) is about the same as the one observed for bare DNA following exposure to H-NS. Furthermore, the time scale of filamentation (hours) is much longer than the one for condensation (minutes). Accordingly, condensation is not related to filamentation per se, but to H-NS mediated attraction of like-charged, distal DNA segments. This is also supported by the downward shift in threshold concentration in the presence of magnesium ions, which are known to promote the formation of H-NS bridges.[64] In a simulation model of DNA compaction by H-NS, it was observed that additional bridges are preferentially formed at sites close to a first bridge.[66] The sigmoidal decrease in extension agrees with such an auto-catalyzed, cooperative reaction of bridge formation, provided the decrease in extension is proportional to the density of bridges. As in the case of the depletion interaction, an effective attractive interaction by bridging ligands requires the juxtaposition of two almost parallel DNA segments.[67] Once the segments are skewed, the contact area is reduced and the attraction disappears. These are the same requirements as for an effective depletion interaction. The nanochannel facilitated condensation by H-NS and the increase in threshold with decreasing channel diameter can hence be explained in terms of the interplay between segment orientation order and juxtaposition as described above for crowded DNA.

Our studies show that the architectural role of H-NS is not only related to its binding modes, but DNA conformation as affected by confinement in a nanospace is of paramount importance. It is the interplay between confinement, H-NS mediated bridging, and filamentation, which controls the conformation and compaction of DNA. Since the typical cross-section of the bacterial nucleoid is a few hundred nm, and comparable with those of our channel systems, we surmise these specific effects play a role in H-NS mediated gene expression regulation and chromosomal organization. In the next section, we will discuss condensation of DNA into a globular form by protamine.

7. Eukaryotic Protamine

Protamines are arginine-rich, cationic proteins that replace histones during spermiogenesis. As a result of this replacement, DNA gets compacted into a condensed, transcriptionally inactive structure.[68] The extent of the compaction depends on the concentration of protamine and the ionic strength of the supporting buffer medium.[69,70] Inspired by its biological relevance, we have done a series of nanofluidics experiments to investigate compaction of DNA by protamine and unpacking of protamine pre-compacted DNA through a change in buffer

conditions.[32] First, we briefly describe the results obtained for pre-incubated DNA inside regular nanochannels. These results will mark the conditions in terms of the range of protamine and salt concentrations for dynamic compaction and unpacking experiments with a cross-channel device to be discussed in the remaining part of this section.

Inside channels with a cross section of $300 \times 200\ nm^2$, we have verified that T4 DNA can be compacted with 0.4 μM of protamine in 1×T buffer. With the addition of 10 mM NaCl to the 1×T buffer, the threshold for compaction decreases about tenfold, to a protamine concentration of 0.03 μM. It should be noted that these threshold concentrations are similar to those discussed above for net electroneutral H-NS. An important difference is that H-NS only facilitates condensation once the molecule is confined in a nanospace, whereas protamine also condenses unconstrained DNA in the bulk phase. In the case of 1×T buffer with 100 mM of added NaCl, no compaction of DNA was observed up to, and including, a protamine concentration of 5 μM. Accordingly, DNA pre-compacted by protamine can subsequently be unpacked with a buffer of high ionic strength.

Protein-free T4 DNA molecules immersed in 1×T buffer were electrophoretically driven into the array of wider nanochannels of the cross-channel device. Once the electric field was removed, the molecules equilibrated and remained stationary inside the wider channels. Since the ionic strength of the buffer was sufficiently low (about 3 mM), the initial stretch of the molecules along the direction of the channel was around 10 μm. Protamine was pipetted into the device and exchanged through the array of narrower channels into the wider channels. Using fluorescence-labeled protamine, it was determined that the buffer exchange was completed within 3 s. A time-lapse series of fluorescence images of T4 DNA, captured after exposure to protamine, as well as the relative extension, are shown in Figure 7A. It is seen that the time scale of compaction depends on the concentration of protamine: the compaction times are 8, 4 and 3 s for 1, 3 and 5 μM protamine, respectively. These times are consistent with the ones reported in the literature for compaction of DNA tethered to optical tweezers in a flow cell.[69] The compaction times for protamine are an order of magnitude shorter than the ones for H-NS. Furthermore, in the case of protamine, the compaction times are somewhat longer than the time required for buffer exchange (3 s), so that a possible sigmoidal decay related to a cooperative binding process could not be detected. Besides compaction time, the final size of the compacted molecules inside the channels depends on the concentration of protamine. For 1, 3 and 5 μM protamine, the compacted molecules have an extension along the channel of 3, 2 and 0.6 μm, respectively. These extensions show that the segment density of the compacted molecules depends on the concentration of the condensing agent.

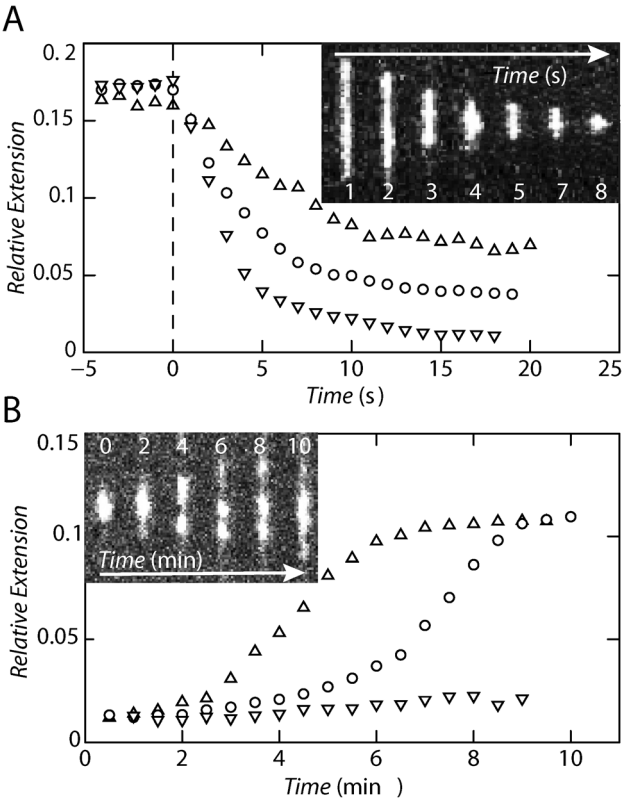

Figure 7. (A) Compaction of T4 DNA following exposure to a solution of 1 (Δ), 3 (○) and 5 (▽) μM protamine in 1×T buffer. The data represent average trajectories pertaining to the compaction of five different molecules. The inset shows a time-lapse series of fluorescence images pertaining to the compaction following exposure to 5 μM protamine in 1×T buffer. Time-zero is defined as the moment when the molecules start to compact. (B) Unpacking of T4 DNA following exposure to a solution of 1 (Δ), 3 (○) and 5 (▽) μM protamine in 1×T buffer and 100 mM NaCl. Prior to unpacking, the DNA molecules were brought into the array of nanochannels in compacted form. The data represent averages pertaining to the unpacking of five different DNA molecules. The inset shows a time-lapse series of fluorescence images pertaining to unpacking following exposure to 1 μM protamine in 1×T buffer and 100 mM NaCl. Panels A and B are reproduced by permission of The Royal Society of Chemistry from Ref. [32].

For a demonstration of the unpacking of DNA pre-compacted with protamine, T4 DNA was incubated with 1 μM protamine in the bulk phase for 24 h. The resulting globules were imaged with atomic force microscopy, and were observed to be toroidal.[68] The globules were electrophoresed into the array of wider channels of the cross-channel device and allowed to equilibrate for at least 10 min. An unpacking buffer containing 1, 3 or 5 μM protamine, 1×T and 100 mM NaCl was exchanged through the narrower, into the wider, channels. The time evolution of the extension following the exchange of buffer is shown in Figure 7B. The initial size of the globules is around 1 μm. Note that the latter size is less than the equilibrated extension obtained for compaction inside

the channels with the same concentration of protamine (3 μm for 1 μM of protamine). This difference in extension shows that the segment density of the compacted molecules depends on confinement during collapse and/or time of incubation. The globules gradually unfold and progressively take a more extended conformation. Compacted substructures typically coexist with unfolded structures, like a beads on a string structure. Furthermore, hints of tails are observed throughout the unpacking process, which indicates the initial unpacking of DNA segments at both ends of the molecule. The unpacking time depends on the concentration of protamine. For 1 and 3 μM protamine, the unpacking times are 8 and 10 min, respectively. In the case of 5 μM protamine, the molecules do not unpack within the time span of our experiment (40 min). Overall, unpacking occurs on a time scale of minutes, which is two orders of magnitude slower than compaction, which occurs on a time scale of seconds.

Overall, the threshold concentrations and final extensions of the condensates for protamine are similar to those obtained for H-NS in the same cross-channel device. Protamine-induced condensation occurs, however, markedly faster, on a time scale of a few seconds. Another important difference is that protamine condenses DNA in the bulk phase, whereas H-NS only facilitates condensation once the molecule is confined in a nanospace. Besides fundamental polymer statistics and protein DNA interaction studies, nanofluidics has found applications in biotechnology. As an example of such a novel application, we will discuss amplification of the stretch by bottlebrush coating DNA with a polypeptide diblock copolymer.

8. Bottlebrush Coating

Nanochannels are important for single-molecule biotechnologies, including the mapping of large-scale genomic organization, restriction enzyme cutting, nick labeling, and denaturation mapping.[21–24,26,27] The resolution of these technologies relies on the ability to stretch DNA to a length close to its contour length. This can be achieved by the confinement of bare DNA inside channels with a diameter of less than the persistence length (50 nm at physiological salt concentrations).[11,22,26] Alternatively, DNA can be stretched by working at very low ionic strength of less than 1 mM.[12–14] At such low ionic strength, the persistence length and effective width of the duplex exceeds 100 and 50 nm, respectively. Following the strategy of amplifying the stretch by an increase in the bending rigidity and width of the duplex, we have applied a polymer coating to the DNA molecule.[33] The advantage of the latter approach is that wider channels can be used, with a diameter of around 250 nm, which can be produced by soft lithography in elastomer. In the next section, we will show that the thus affected amplified stretch is sufficient to map large-scale genomic organization.

A suitable polymer for coating of DNA is the cationic-neutral diblock polypeptide C_4K_{12}.[71] The cationic binding block consists of 12 lysine residues (K_{12}). The K_{12} block is coupled to 4 repeats of a 100 amino acid long polypeptide (C_4). The C_4 block has an amino acid composition similar to that of collagen and behaves as a flexible polymer in aqueous solution. The polypeptide is monodisperse, with a molecular weight of 38.4 kDa. The polypeptide concentration is expressed as the N/P ratio; that is, the number of positively charged amino groups on the lysine K_{12} binding block divided by the number of phosphate groups on the DNA. Single DNA molecules are uniformly coated through binding of the cationic K_{12} block, as illustrated in Figure 8A. The persistence lengths and widths of the bottlebrush complexes were obtained from analysis of atomic force microscopy images.[72] A typical image of linearized pUC18 plasmid (2686 bp), coated with C_4K_{12} with N/P = 2.0 and adsorbed on silica, is shown in Figure 8B (the relatively small plasmids are imaged in their entirety). With increasing C_4K_{12} to DNA ratio, the persistence length, *P*, increases from 60 nm (bare DNA) to 240 nm at the highest polypeptide concentration. The atomic force microscopy images also show an increase in the width of

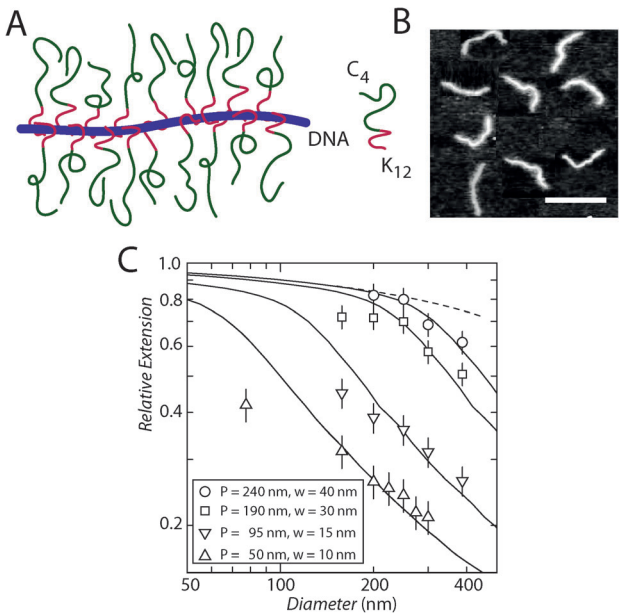

Figure 8. (A) Drawing of a bottlebrush, formed by binding a diblock polypeptide copolymer to DNA. The binding block of the copolymer contains 12 cationic lysine residues. The neutral block is collagen-like. (B) Montage of tapping mode atomic force microscopy images of linearized pUC18 DNA complexed with polypeptide with N/P = 2.0. The scale bar denotes 1 μm. (C) Relative extension of T4 DNA in 1×T. The N/P ratios are 0 (Δ), 0.1 (▽),1.0 (□) and 2.0 (○). The solid curves are Monte Carlo results, with noted values of persistence length, *P*, and width, *w*. The dashed curve represents deflection theory for narrow channels. The panels are reproduced by permission of Oxford University Press from Ref. [33].

the bottlebrushes. Gaussian fits of the cross-sectional profiles give variances of 10, 15, 20, and 30 nm for N/P = 0, 0.1, 1.0, and 2.0, respectively. The latter values are merely indicative, because the brushes are dried and spread out on the surface.

Coated and stained T4 DNA molecules were electrophoresed into the nanochannels, equilibrated, and imaged with fluorescence microscopy. The relative extensions are set out in Figure 8C. With decreasing channel diameter and/or increasing C_4K_{12} to DNA ratio, the relative extension increases. For N/P = 0 (polypeptide-free) and 0.1, the extensions are in the range 0.2–0.5 times the contour length. In the case of N/P ratios of 1.0 and 2.0, the relative extensions are in the range 0.5–0.85. Furthermore, the extensions level off at a plateau value for smaller channel diameters and higher N/P ratios. Note that with a twofold excess of polypeptide to DNA charge (N/P = 2.0), the stretch reaches about 85% of the contour length. To quantify the stretch in terms of persistence length, *P*, and effective width, *w*, the experimental values can be compared with Monte Carlo results. The computational results are also displayed in Figure 8C. In comparing the experimental values with the Monte Carlo results, we have used the values of the persistence length, *P*, as obtained from atomic force microscopy (for bare DNA we have used the nominal value *P* = 50 nm). For each N/P ratio, the width, *w*, used in the Monte Carlo simulations was adjusted to obtain the best agreement with the stretching data. The values of *w* obtained in this way show an increase with increased polypeptide coating and are in reasonable agreement with the variances of the cross-sectional profiles obtained from atomic force microscopy. Overall, the stretch agrees with the simulation results, and confirms the transition from the blob to the deflection regime, with increased coating of the DNA molecule. In the next section, we will show that bottlebrush coating can be used to linearize DNA for mapping of large-scale genomic organization.

9. Large-scale Genome Mapping

The aim of large-scale genome mapping is not to determine the genetic code at the single base level, but rather to provide a map for assembling the genome at the larger scale, and to sort out large-scale variations such as insertions, inversions, and translocations. To achieve the necessary resolution of less than 2 kbp, the molecules need to be stretched to a length close to their contour length. For bare DNA in physiological buffer conditions, this requires rather narrow 45 nm channels which are usually made of fused silica.[22,24] Alternatively, DNA molecules can be stretched by coating them with polypeptide diblock copolymer. As described above, a maximum stretch of 85% of the contour length can be obtained for N/P = 2.0 in 150 × 250 nm^2 channels, produced by soft lithography in elastomer. Here, we will show that this amplification of the stretch in tandem with site-specific fluorescence labeling allows the investigation of large-scale genomic organization.[33]

For a demonstration of the genome mapping technology, site-specific nicks of λ DNA (48.5 kbp) are labeled with Alexa Fluor 546.[22,24] There are four resolvable labeling sites at 8, 18.3 (average of two sites at 18.1 and 18.5 kbp), 31.3 (average of 30.9, 31.2, and 31.8 kbp), and 35.8 kbp. Furthermore, the sticky ends of the λ DNA molecule can also be labeled. The YOYO-1 and Alexa-labeled DNA was coated with C_4K_{12} and brought into nanochannels with a cross-sectional diameter of 150 × 250 nm^2. As can be seen in Figure 9A, individual Alexa labels are discernible with an N/P ratio of 2.0. Individual labels can also be discerned for N/P = 1.0, albeit with decreased separation. In the case of polypeptide-free DNA, individual labeled sites cannot be discerned (images for N/P = 0 and 1.0 are not shown). This confirms that an excess of polypeptide is needed to achieve the highest possible stretch. The Alexa labeling procedure is not perfect, because occasionally, labels are missing (in particular, the ones at the end). Out of a pool of 100 molecules, 2, 10, and 40% of the molecules show 6, 5, and 4 discernible labels, respectively. The problem of missing labels can be alleviated by analyzing a larger pool of molecules. Single-molecule Alexa profiles of 50 molecules were aligned and corrected for a minor variation in overall stretch of less than 5%. The locations of corresponding labels for different molecules are in register. As shown by the average profile in Figure 9B, the locations of the labels along the molecule are in good agreement with the locations of the nicking sites. Accordingly, the molecules are uniformly stretched along the direction of the channel without ever folding back. The resolution in peak position is around 2 kbp, which is similar to the one reported for bare DNA in 45 nm channels.[22,24]

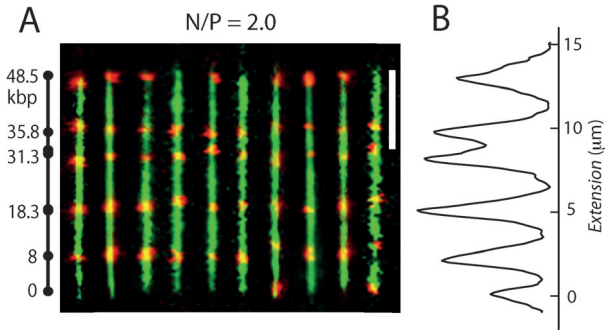

Figure 9. (A) Montage of fluorescence images of λ DNA. The images obtained with YOYO-1 (green) and Alexa Fluor 541 (red) staining are superposed. The molecules are confined in 150 × 250 nm^2 channels with N/P = 2.0. labeling sites are noted. The scale bar denotes 5 μm. (B) Average Alexa profile over a pool of 50 molecules. The panels are reproduced by permission of Oxford University Press from Ref. [33].

10. Outlook

Although significant progress has been made, nanofluidics still has a lot of potential for new developments in fundamental science and technology. One can identify a number of promising fields of research, of which we will mention a few. Most of the existing studies involve the confinement of DNA in linear form. However, *in vivo*, DNA is often, if not always, closed circular and supercoiled. The interplay of nano-confinement and supercoiling is also of importance for the compaction of DNA in a congested state. As in the case of other modes of compaction, such as macromolecular crowding or bridging by architectural protein, this could be investigated with a nanofluidics platform.[73] Yet, nanofluidic studies on closed circular DNA, such as bacterial artificial chromosomes, are scarce.[10] With the maturing of the technology, including the possibility of modulation of degree of supercoiling by topology-controlling enzymes (topoisomerases) inside the channel system, this situation could change in the not too distant future. Another interesting development is the utilization of nanofluidic devices for DNA binding assays, if the accessibility of binding ligands and/or proteins to channel-confined DNA is preserved (as in the case of our cross channel device). For a better understanding of DNA metabolism, a larger pool of proteins and ligands can then be investigated, including the ones that bind at a specific site of the DNA molecule.

As we have discussed above, existing single-molecule sequencing technologies aim at resolving large-scale genomic information (kilo base-pair scale). The development of cheap, polymer-based biochips, possibly in conjunction with other stretching methodologies such as bottlebrush coating, will reduce cost and make these technologies available to a larger community. An exciting new development is the integration of single-nucleobase sensing technologies in lab-on-chip devices. In such a device, a strand of DNA is threaded through or along a sensor to sequence it at the level of individual nucleobases. In recent years, progress has been made in the sequencing of DNA by nanopores and nanoribbons, with a strong indication that individual nucleotides can be resolved.[74–76] However, to fulfill the main promise of nanopore or ribbon sequencing technologies, i.e., single-molecule sequencing of the genome from a single cell without polymer chain reaction amplification and with single nucleobase resolution, the genetic material has to be collected, sorted, directed, and read out with an integrated lab-on-chip device. A major challenge is hence the development of such micro/nanofluidic devices, which will greatly enhance their performance by pushing the resolution from the kilo to single nucleobase level.

Besides the genetic code encoded in Watson-Crick base pairing, the heritable phenotype is controlled by epigenetic mechanisms. Examples of these mechanisms are DNA methylation and histone modification. They do not only regulate the expression of genes and cell differentiation, but also their deregulation, causing detrimental cell functionality and disease. Methods to rapidly assess the epigenetic profile of differentiated and/or diseased cells are hence of critical importance in a variety of biological and biomedical applications. A promising novel epigenetic profiling technology is based on a platform of nanofluidic channels. As in the case of bare DNA, the nucleic content of the cell nucleus (chromatin) can be stretched and linearized on an array of nanochannels.[77–79] An epigenetic profile of, for instance, methylated histone, H3, and acetylated histone, H4, along the linearized chromatin complex can then be obtained by histone-specific binding of fluorescence-labeled antibodies. Besides modified histones, it is also possible to obtain a profile of cytosine methylation.[80] To relate the epigenetic profile to the gene sequence, it is desirable to use an integrated micro/nanofluidic device that allows read out of epigenetic and genetic information from the same material extracted from a single cell.

Acknowledgements

This work has been supported by FRC grants R-144-000-312-112, R-144-000-336-112, and MOE Academic Research Fund MOE2009-T2-2-005. The authors thank L. Dai, S. Y. Ng, J. J. Jones, P. S. Doyle, P. P. Malar, Z. Gong, D. Guttula, F. Liu, K. Jiang, A. Hernandez-Garcia, S. Garaj, R. de Vries, and V. Arluison for their contributions, discussions, and support.

References

[1] G. W. Slater, Y. Gratton, M. Kenward, L. McCormick, F. Tessier, *Soft Matter* **2003**, *1*, 365.
[2] J. Han, H. G. Craighead, *Science* **2000**, *288*, 1026.
[3] N. Kaji, Y. Tezuka, Y. Takamura, M. Ueda, T. Nishimoto, H. Nakanishi, Y. Horiike, Y. Baba, *Anal. Chem.* **2004**, *76*, 15.
[4] J. L. Li, M. Gershow, D. Stein, E. Brandin, J. A. Golovchenko, *Nat. Mater.* **2003**, *2*, 611.
[5] C. Bustamante, J. F. Marko, E. Siggia, S. Smith, *Science* **1994**, *265*, 1599.
[6] C. G. Baumann, S. B. Smith, V. A. Bloomfield, C. Bustamante, *Proc. Natl. Acad. Sci. U.S.A.* **1997**, *94*, 6185.
[7] M. C. Williams, *Proc. Natl. Acad. Sci. U.S.A.* **2007**, *104*, 11125.
[8] S. Jun and B. Mulder, *Proc. Natl. Acad. Sci. U.S.A.* **2006**, *103*, 12388.
[9] W. Reisner, K. J. Morton, R. Riehn, Y. M. Wang, Z. Yu, M. Rosen, J. C. Sturm, S. Y. Chou, E. Frey, R. H. Austin, *Phys. Rev. Lett.* **2005**, *94*, 196101.
[10] F. Persson, P. Utko, W. Reisner, N. B. Larsen, A. Kristensen, *Nano Lett.* **2009**, *9*, 1382.
[11] W. Reisner, J. P. Beech, N. B. Larsen, H. Flyvbjerg, A. Kristensen, J. O. Tegenfeldt, *Phys. Rev. Lett.* **2007**, *99*, 058302.

[12] K. Jo, D. M. Dhingra, T. Odijk, J. J. de Pablo, M. D. Graham, R. Runnheim, D. Forrest, D. C. Schwartz, *Proc. Natl. Acad. Sci. U.S.A.* **2007**, *104*, 2673.
[13] C. Zhang, F. Zhang, J. A. van Kan, J. R. C. van der Maarel, *J. Chem. Phys.* **2008**, *128*, 225109.
[14] Y. Kim, K. S. Kim, K. L. Kounovsky, R. Chang, G. Y. Jung, J. J. de Pablo, K. Jo, D. C. Schwartz, *Lab Chip* **2011**, *11*, 1721.
[15] J. O. Tegenfeldt, C. Prinz, H. Cao, S. Chou, W. W. Reisner, R. Riehn, Y. M. Wang, E. C. Cox, J. C. Sturm, P. Silberzan, R. H. Austin, *Proc. Natl. Acad. Sci. U.S.A.* **2004**, *101*, 10979.
[16] J. T. Mannion, C. H. Reccius, J. D. Cross, H. G. Craighead, *Biophys J.* **2006**, *90*, 4538.
[17] P. Cifra, Z. Benkova, T. Bleha, *J. Phys. Chem. B* **2008**, *112*, 1367.
[18] Y. Wang, D. R. Tree, K. D. Dorfman, *Macromolecules* **2011**, *44*, 6594.
[19] P. Cifra, *J. Chem. Phys.* **2012**, *136*, 024902.
[20] L. Dai, J. J. Jones, J. R. C. van der Maarel, P. S. Doyle, *Soft Matter* **2012**, *8*, 2972.
[21] R. Riehn, M. Lu, Y. M. Wang, S. F. Lim, E. C. Cox, R. H. Austin, *Proc. Natl. Acad. Sci. U.S.A.* **2005**, *102*, 10012.
[22] S. K. Das, M. D. Austin, M. C. Akana, P. Deshpande, H. Cao, M. Xiao, *Nucleic Acids Res.* **2010**, *38*, e177.
[23] W. Reisner, N. B. Larsen, A. Silahtaroglu, A. Kristensen, N. Tommerup, J. O. Tegenfeldt, H. Flyvbjerg, *Proc. Natl. Acad. Sci. U.S.A.* **2010**, *107*, 13294.
[24] E. T. Lam, A. Hastie, C. Lin, D. Ehrlich, S. K. Das, M. D. Austin, P. Deshpande, H. Cao, N. Nagarajan, M. Xiao, P. Y. Kwok, *Nat. Biotechnol.* **2012**, *30*, 771.
[25] S. K. Min, W. Y. Kim, Y. Cho, K. S. Kim, *Nat. Nanotechnol.* **2011**, *6*, 162.
[26] S. L. Levy, H. G. Craighead, *Chem. Soc. Rev.* **2010**, *39*, 1133.
[27] W. Reisner, J. N. Pedersen, R. H. Austin, *Rep. Prog. Phys.* **2012**, *75*, 106601.
[28] J. A. van Kan, C. Zhang, P. P. Malar, J. R. C. van der Maarel, *Biomicrofluidics* **2012**, *6*, 036502.
[29] C. Zhang, P. G. Shao, J. A. van Kan, J. R. C. van der Maarel, *Proc. Natl. Acad. Sci. U.S.A.* **2009**, *106*, 16651.
[30] C. Zhang, Z. Gong, D. Guttula, P. P. Malar, J. A. van Kan, P. S. Doyle, J. R. C. van der Maarel, *J. Phys. Chem. B* **2012**, *116*, 3031.
[31] C. Zhang, D. Guttula, F. Liu, P. P. Malar, S. Y. Ng, L. Dai, P. S. Doyle, J. A. van Kan, J. R. C. van der Maarel, *Soft Matter* **2013**, *9*, 9593.
[32] C. Zhang, K. Jiang, F. Liu, P. S. Doyle, J. A. van Kan, J. R. C. van der Maarel, *Lab Chip* **2013**, *13*, 2821.
[33] C. Zhang, A. Hernandez-Garcia, K. Jiang, Z. Gong, D. Guttula, S. Y. Ng, P. P. Malar, J. A. van Kan, L. Dai, P. S. Doyle, R. de Vries, J. R. C. van der Maarel, *Nucleic Acids Res.* **2013**, *41*, e189.
[34] J. A. van Kan, A. A. Bettiol, F. Watt, *Appl. Phys. Lett.* **2003**, *83*, 1629.
[35] J. A. van Kan, A. A. Bettiol, F. Watt, *Nano Lett.* **2006**, *6*, 579.
[36] Y. Yao, P. Santhanan Raman, J. A. van Kan, *Microsyst. Technol.* **2014**, *20*, 2065.
[37] J. A. van Kan, P. G. Shao, Y. H. Wang, P. P. Malar, *Microsyst. Technol.* **2011**, *17*, 1519.
[38] H. P. Spielmann, D. E. Wemmer, J. P. Jacobsen, *Biochemistry* **1995**, *34*, 8542.
[39] F. Johansen, J. P. Jacobsen, *J. Biomol. Struct. Dyn.* **1998**, *16*, 205.
[40] J. R. C. van der Maarel, *Introduction to Biopolymer Physics*, World Scientific, Singapore, **2008**.
[41] M. Daoud, P. G. de Gennes, *J. Phys.* **1977**, *38*, 85.
[42] P. G. de Gennes, *Scaling Concepts in Polymer Physics*, Cornell University Press, Ithaca, **1979**.
[43] T. Odijk, *Macromolecules* **1983**, *16*, 1340.
[44] R. Riehn, R. H. Austin, J. C. Sturm, *Nano Lett.* **2006**, *6*, 1973.
[45] T. Su, S. K. Das, M. Xiao, P. K. Purohit, *PLoS One* **2011**, *6*, e16890.
[46] Y. Z. Yang, T. W. Burkhardt, G. Gompper, *Phys. Rev. E: Stat. Nonlinear Soft Matter Phys.* **2007**, *76*, 011804.
[47] L. Dai, J. R. C. van der Maarel, P. S. Doyle, *Macromolecules* **2014**, *47*, 2445.
[48] T. Odijk, *J. Chem. Phys.* **2006**, *125*, 204904.
[49] T. Odijk, *Phys. Rev. E: Stat. Nonlinear Soft Matter Phys.* **2008**, *77*, 060901(R).
[50] L. Dai, S. Y. Ng, P. S. Doyle, J. R. C. van der Maarel, *ACS Macro Lett.* **2012**, *1*, 1046.
[51] L. S. Lerman, *Proc. Natl. Acad. Sci. U.S.A.* **1971**, *68*, 1886.
[52] V. A. Bloomfield, *Curr. Opin. Struct. Biol.* **1996**, *6*, 334.
[53] M. Kojima, K. Kubo, K. Yoshikawa, *J. Chem. Phys.* **2006**, *124*, 024902.
[54] H. Walter, D. E. Brooks, *FEBS Lett.* **1995**, *361*, 135.
[55] S. B. Zimmerman, L. D. Murphy, *FEBS Lett.* **1996**, *390*, 245.
[56] J. J. Jones, J. R. C. van der Maarel, P. S. Doyle, *Nano Lett.* **2011**, *11*, 5047.
[57] S. Asakura, F. Oosawa, *J. Chem. Phys.* **1955**, *22*, 1255.
[58] R. de Vries, *J. Chem. Phys.* **2006**, *125*, 014905.
[59] U. Bohme, U. Scheler, *Chem. Phys. Lett.* **2007**, *435*, 342.
[60] D. F. Browning, D. C. Grainger, S. J. W. Busby, *Curr. Opin. Microbiol.* **2010**, *13*, 773.
[61] R. Amit, A. B. Oppenheim, J. Stavans, *Biophys. J.* **2003**, *84*, 2467.
[62] E. Bouffartigues, M. Buckle, C. Badaut, A. Travers, S. Rimsky, *Nat. Struct. Mol. Biol.* **2007**, *14*, 441.
[63] C. L. Woldringh, N. Nanninga, *J. Struct. Biol.* **2006**, *156*, 273.
[64] R. T. Dame, C. Wyman, N. Goosen, *Nucleic Acids Res.* **2000**, *28*, 3504.
[65] Y. Liu, H. Chen, L. J. Kenney, J. Yan, *Genes Dev.* **2010**, *24*, 339.
[66] M. Joyeux, J. Vreede, *Biophys. J.* **2013**, *104*, 1615.
[67] L. Dai, Y. Mu, L. Nordenskiöld, J. R. C. van der Maarel, *Phys. Rev. Lett.* **2008**, *100*, 118301.
[68] M. J. Allen, E. M. Bradbury, R. Balhorn, *Nucleic Acids Res.* **1997**, *25*, 2221.
[69] L. R. Brewer, M. Corzett, R. Balhorn, *Science* **2005**, *286*, 120.
[70] N. Makita, Y. Yoshikawa, Y. Takenaka, T. Sakaue, M. Suzuki, C. Watanabe, T. Kanai, T. Kanbe, T. Imanaka, K. Yoshikawa, *J. Phys. Chem. B.* **2011**, *115*, 4453.
[71] A. Hernandez-Garcia, M. W. Werten, M. C. Stuart, F. A. de Wolf, R. de Vries, *Small* **2012**, *8*, 3491.
[72] P. A. Wiggins, T. van der Heijden, F. M. Herrero, A. Spakowitz, R. Phillips, J. Widom, C. Dekker, P. C. Nelson, *Nat. Nanotechnol.* **2006**, **1**, 137.
[73] W. Lim, S. Y. Ng, C. Lee, Y. P. Feng, J. R. C. van der Maarel, *J. Chem. Phys.* **2008**, *129*, 165102.
[74] D. Branton, D. W. Deamer, A. Marziali, H. Bayley, S. A. Benner, T. Butler, M. Di Ventra, S. Garaj, A. Hibbs, X. Huang, S. B. Jovanovich, P. S. Krstic, S. Lindsay, X. S. Ling, C. H. Mastrangelo, A. Meller, J. S. Oliver, Y. V. Pershin, J. M. Ramsey, R. Riehn, G. V. Soni, V. Tabard-Cossa, M.

Wanunu, M. Wiggin, J. A. Schloss, *Nat. Biotechnol.* **2008**, *26*, 1146.
[75] S. Garaj, W. Hubbard, A. Reina, J. Kong, D. Branton, J. A. Golovchenko, *Nature* **2010**, *467*, 190.
[76] B. M. Venkatesan, R. Bashir, *Nat. Nanotechnol.* **2011**, *6*, 615.
[77] B. R. Cipriany, R. Zhao, P. J. Murphy, S. L. Levy, C. P. Tan, H. G. Craighead, P. D. Soloway, *Anal. Chem.* **2010**, *82*, 2480.
[78] T. Matsuoka, B. C. Kim, J. Huang, N. J. Douville, M. D. Thouless, S. Takayama, *Nano Lett.* **2012**, *12*, 6480.
[79] T. Matsuoka, B. C. Kim, C. Moraes, M. Hun, S. Takayama, *Biomicrofluidics* **2013**, *7*, 041301.
[80] P. J. Murphy, B. R. Cipriany, C. B. Wallin, C. Y. Ju, K. Szeto, J. A. Hagarman, J. J. Benitez, H. G. Craighead, P. D. Soloway, *Proc. Natl. Acad. Sci. U.S.A.* **2013**, *110*, 7772.

Received: May 29, 2014
Accepted: July 7, 2014
Published online: ■■ ▮▮, 0000

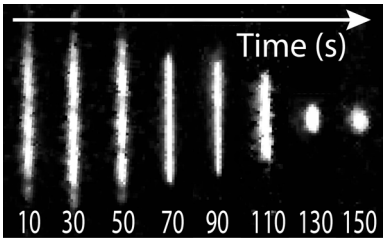

J. R. C. van der Maarel, C. Zhang, J. A. van Kan*

■■–■■

A Nanochannel Platform for Single DNA Studies: From Crowding, Protein DNA Interaction, to Sequencing of Genomic Information